Accepted Manuscript

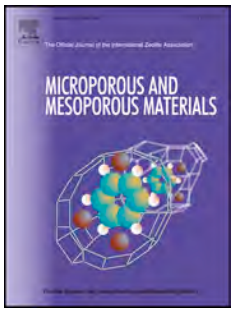

Homogeneous thin coatings of zeolitic imidazolate frameworks prepared on quartz crystal sensors for CO_2 adsorption

Lilian Sarango, Javier Benito, Ignacio Gascón, Beatriz Zornoza, Joaquín Coronas

PII: S1387-1811(18)30328-7

DOI: 10.1016/j.micromeso.2018.06.018

Reference: MICMAT 8971

To appear in: *Microporous and Mesoporous Materials*

Received Date: 6 April 2018

Revised Date: 6 June 2018

Accepted Date: 9 June 2018

Please cite this article as: L. Sarango, J. Benito, I. Gascón, B. Zornoza, Joaquí. Coronas, Homogeneous thin coatings of zeolitic imidazolate frameworks prepared on quartz crystal sensors for CO_2 adsorption, *Microporous and Mesoporous Materials* (2018), doi: 10.1016/j.micromeso.2018.06.018.

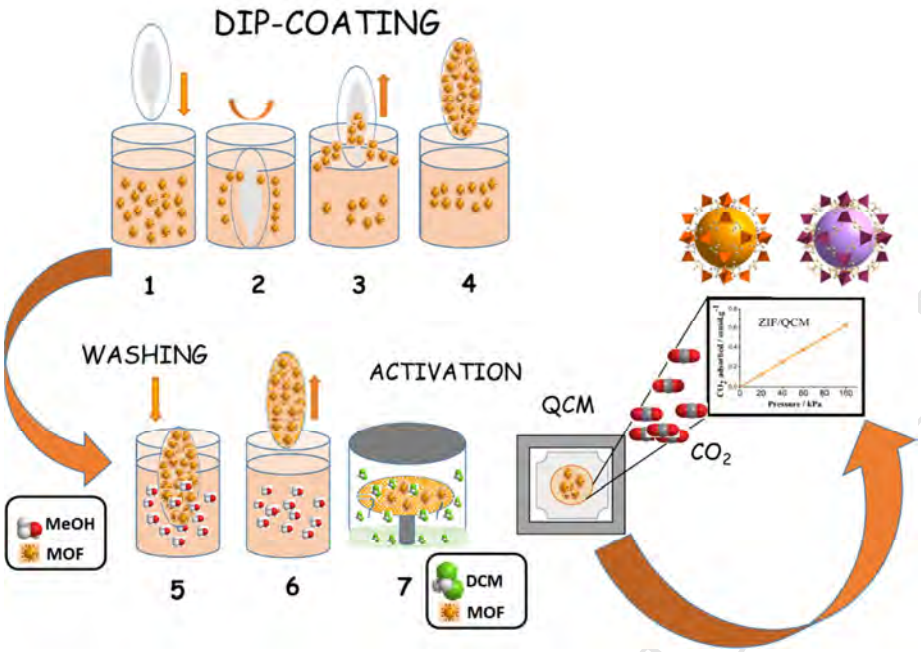

Homogeneous thin coatings of zeolitic imidazolate frameworks prepared on quartz crystal sensors for CO_2 adsorption

Lilian Sarango,[a,b] Javier Benito,[c] Ignacio Gascón,[c] Beatriz Zornoza,[a] and Joaquín Coronas[a,*]

[a]Chemical and Environmental Engineering Department and Instituto de Nanociencia de Aragón (INA), Universidad de Zaragoza, 50018 Zaragoza, Spain

[b]Electronics Engineering Career, Salesian Polytechnic University, Cuenca, Ecuador

[c]Departamento de Química Física, Facultad de Ciencias, and Instituto de Nanociencia de Aragón (INA), Universidad de Zaragoza, 50018 Zaragoza, Spain

*Corresponding author: coronas@unizar.es

Abstract

Thin films of four zeolitic-imidazolate frameworks (ZIF-8, ZIF-67, ZIF-7, and ZIF-93) have been fabricated by a dip-coating method on glass and quartz crystal microbalance (QCM) substrates obtaining homogeneous coatings with sizes of nanoparticles of 65±20, 285±96, 61±20 and 72±21 nm for ZIF-8, ZIF-67, ZIF-7, and ZIF-93, respectively. Upon characterization of the ZIFs and coatings by XRD, TGA, SEM, FTIR, contact angle measurement and N_2 adsorption, the coatings were exposed to vapors of dichloromethane for activation. The CO_2 adsorption of the coatings was then studied using a QCM device.

Keywords: Metal-organic framework; Zeolitic imidazolate framework; Dip-coating; Quartz crystal microbalance; CO_2 adsorption.

1. Introduction

Zeolitic imidazolate frameworks (ZIFs) are a subclass of metal–organic frameworks (MOFs) with imidazolate type ligands [1]. ZIFs are porous crystalline solids in which tetrahedral divalent metal ions (M= Zn^{2+}, Co^{2+}) are connected via coordination bonds to an imidazole derivative (Im) [1, 2]. The fact that the M-Im-M angle is similar to the Si-O-Si angle (145°) in zeolites has led to the synthesis of a large number of ZIFs with zeolite-type tetrahedral topologies [3]. ZIFs exhibit permanent porosity and high thermal and chemical stabilities, which make them attractive materials for application in diverse fields such as catalysis [4], biomedicine [5, 6], gas separation [7, 8], organic solvent nanofiltration [9, 10], chemical sensing [11] and imaging [12]. The versatile properties of ZIFs also make them good candidates for use as sensing material hosts [13, 14]. Lu and Hupp [15] reported the fabrication of ZIF-8 films on a Fabry–Pérot device for gas and vapor detection. Tu et al. [16] prepared ZIF thin film devices for selective detection of volatile organic compounds (VOCs).

The ZIFs studied in this work (ZIF-8, ZIF-67, ZIF-7 and ZIF-93) were selected for their small pore sizes, high chemical stability and ease of preparation as nanoparticles. ZIF-8 [2] and ZIF-67 [1] have cubic structures having the same organic linker, 2- methylimidazolate (mIm), coordinated with Zn(II) and Co(II) cations, respectively. Both ZIFs have micropores related to the **sod** type topology with cavity diameters of 1.16 nm accessible through small pore windows of 0.34 nm diameter. ZIF-7 [17] shares the same metal ion (Zn) and **sod** type topology as ZIF-8 but its crystal structure is different: ZIF-8 exhibits a cubic structure, while ZIF-7 has a trigonal symmetry in a trigonal space group with benzimidazolate (bIm) as linker [16]. ZIF-93

[18] exhibits the **rho** topology and forms crystals with a cubic space group but is constructed by the coordination of metal ion (Zn) with 4-imidazolate-5-carboxyaldehyde (4m5ImCA).

The deposition of MOF thin films on various surfaces using different methods has been previously reported as the first step towards the permanent placing of MOFs for device fabrication. In consequence, the control of the technology of MOF positioning is of paramount importance for device fabrication [19]. Therefore, several strategies have been developed to prepare MOF thin films. Layer-by-layer [19], direct growth [15], Langmuir-Blodgett method [20], pulsed-laser deposition, chemical vapor deposition [21], and spray method [22, 23] can be mentioned among the suitable technologies for the purpose of MOF controlled deposition. However, some of them may produce a poor control of thickness and morphology [24], or are highly time-consuming [25]. In this work, it has been used the dip-coating method, previously reported for MOFs showing that they retain their intrinsic properties upon the application of the technique [10, 26, 27]. This method is simple, scalable on large surfaces and can be adapted to the deposition of a wide range of colloidal materials such as polymers, inorganic materials and hybrid particles [10, 28, 29]. More importantly, dip-coating deposition permits a high degree of control over the thickness and layer structure through the mastering of the withdrawal speed [30]. One of the most direct applications of MOF thin films is the coating of gold coated quartz-substrates, such as quartz crystal microbalances (QCM) used as sensors. A QCM sensor is a useful tool for detecting mass changes at the sensing surface in real time [31]. Recently, QCM sensors have been applied to measure the mass change related to MOF films [16, 32-34]. Here, we propose a rapid and inexpensive method of dip-coating at room temperature to fabricate thin films, simply by immersing glass or QCM substrates

previously cleaned and functionalized in a ZIF suspension. The films obtained were activated by exchanging the remaining synthesis solvent (MeOH) with dichloromethane vapor [35]. CO_2 adsorption of the ZIF coatings was studied by using a QCM device.

2. Experimental Section

2.1. Materials

$Zn(NO_3)_2 \cdot 6H_2O$ (99% purity, Sigma Aldrich), 2-methylimidazole (mIm) (99% purity, Scharlab), $Co(NO_3)_2 \cdot 6H_2O$ (99% purity, Sigma Aldrich), methanol (99% purity, Scharlab), benzimidazole (bIm) (99% purity, Scharlab), 4-methyl-5-imidazolecarboxaldehyde (4m5ImCA) (99% purity, Sigma Aldrich), H_2O_2 (30% purity, Sigma Aldrich), H_2SO_4 (95-98% purity, Sigma Aldrich), dichloromethane (DCM) (99% purity, Sigma Aldrich), 2-[methoxy(polyethyleoxy)propyl]trichlorosilane (relative density 1.13) (PEG silane, Fluorochem) and alpha-methoxy-omega-mercapto (MeO-PEG-SH, 2000 Da, Iris Biotech) were used as received without further purification.

2.2. Synthesis of ZIFs

ZIF-8 was synthesized based on the methodology reported elsewhere [36]. The following molar composition was used: 1 Zn: 8 mIm: 700 MeOH. $Zn(NO_3)_2 \cdot 6H_2O$ (1.41 g) and mIm (3.1 g) were separately dissolved in 67 mL of methanol each. Then the solution of the ligand was poured on that of the metal salt and the resulting solution was stirred for 20 min at room temperature. This produced a white dispersion containing ZIF-8.

ZIF-67 synthesis was based on the previously reported molar composition [10]: 1 Co: 8 mIm : 700 MeOH. $Co(NO_3)_2 \cdot 6H_2O$ (1.41 g) and mIm (3.1 g) were separately

dissolved in 68.5 mL of methanol each. Then the solution of the ligand was poured on that of the metal salt and the resulting solution was stirred for 20 min at room temperature. A purple coloration indicated the formation of ZIF-67.

ZIF-93 was synthesized based on the methodology reported elsewhere [37], with an adaptation to the following molar composition: 1 Co: 8 4m5ImCA : 3000 MeOH (from 1:8:1000). $Zn(NO_3)_2 \cdot 6H_2O$ (0.88 g) and 4m5ImCA (2.6 g) were separately dissolved in 131 mL of methanol each. Then the solution of the ligand was poured on that of the metal salt and the resulting solution was stirred for 20 min at room temperature. This produced a beige dispersion containing ZIF-93.

ZIF-7 was synthesized following a previously reported method with the following molar composition [38]: 1 Zn: 6 bIm: 120 DMF. Zn $(NO_3)_2 \cdot 6H_2O$ (0.64 g) and bIm (1.63 g) were separately dissolved in 100 mL of DMF each. Then the solution of the ligand was poured on that of the metal salt and the resulting solution was stirred for 48 h at room temperature. A white coloration indicated the formation of ZIF-7.

The precipitates of ZIF-8, ZIF-67, and ZIF-93 were collected by centrifugation and washed with methanol 3 times. ZIF-7 was washed once with DMF and twice with methanol, and the product obtained was exchanged with methanol during 24 h to remove DMF. Finally, all the ZIFs were dispersed in methanol until the desired concentration for the dip-coating process.

2.3 Sample preparation

Glass substrates (18 x 18 mm, 3.24 cm^2 square cover glasses) were washed with acetone and 2-propanol in an ultrasound bath to remove grease and traces of other possible organic impurities from their surface, and then dried under nitrogen flow. After that, the substrates were immersed in piranha solution (3:1 sulfuric acid: hydrogen

peroxide) for 30 min, rinsed several times with deionized water (Millipore water purification system) and dried under nitrogen flow. Piranha solution is very corrosive, reactive and potentially explosive and should be handled with care. This cleaning procedure allows terminal hydroxyl groups to be obtained, which are necessary for the subsequent functionalization. In order to obtain PEG terminated surfaces, the substrates were placed in 1 % (v/v) solution of PEG silane in anhydrous toluene for 1 h and 30 min at room temperature. After rinsing each sample with the ethanol, the samples were dried under nitrogen flow and kept in a desiccator.

Prior to modification, the QCM substrates were cleaned with the above described piranha solution for 1 min, followed by thorough rinsing with deionized water. For the functionalization, the QCMs were placed in a 0.05 M solution of MEO-PEG-SH in water during 24 h. A more specific reagent with thiol groups was used for the functionalization of the QCM substrates metalized with gold electrodes. The QCMs were then rinsed with ethanol, dried under nitrogen flow and kept in a desiccator.

2.4 Coating of ZIF onto glass support by dip-coating

Glass substrates were immersed vertically for dip-coating into ZIF (ZIF-8, ZIF-67, ZIF-7 and ZIF-93) suspensions with ZIF concentrations in the range of 0.007-0.01 $g \cdot mL^{-1}$. A constant speed of 40 $mm \cdot min^{-1}$ was used for the entry of the glass substrate into the ZIF suspension followed by a 10 min immersion time. Then, the substrate was removed from the ZIF suspension at the same 40 $mm \cdot min^{-1}$ speed and washed with methanol for 5 s. All the process was carried out at the controlled temperature of 20±1 °C and ca. 40% of relative humidity. The total time of the film preparation (in principle, a ZIF monolayer) is 14 min. The substrates with the ZIF monolayer were dried at 65 ºC overnight giving rise to ZIF-coated supports, named ZIF/glass_1L. The name

ZIF/glass_2L was used for twice coated supports, repeating immediately the procedure described above before washing and drying. For the purpose of characterization, the remaining ZIFs in their corresponding used suspensions were collected by repeated centrifugation (12000 rpm and 15 min), rinsed with methanol (3x) and dried overnight at 65° C. ZIF-7 was dried at 140 °C due to the use of a higher boiling point solvent DMF in its synthesis.

2.5 Coating of ZIF onto QCM Substrates by dip-coating

Following the same procedure as described above for coating glass substrates (except for the drying step), the QCM substrates were subjected to dip-coating in a suspension of the ZIF under study at a concentration of 0.007-0.01g·mL^{-1}. In this case, only 2-4 layers were deposited. The deposition system (KSV Minimicro) consists of a DC motor controlled to ensure vibration-free operation. The speed range of the dipping arm is 0.1-85 mm/min and the maximum stroke is about 75 mm. The position is determined with an optical encoder. The deposition system is equipped with safety switches which stop the motor automatically at both ends. For activation of ZIF, the coated QCM was exposed in a recipient to DCM vapor for 12 h at room temperature. The recipient contained 6 mL of DCM(l) so that the liquid was not in direct contact with the QCM, and was sealed with paraffin. The idea was to exchange solvents in the vapor phase (methanol, boiling point 64.7 ºC, by DCM, boiling point 39.6 ºC). Then DCM would be easily removed from the QCM at the limited activation temperature that the QCM system can withstand due to the electronics (70-80 ºC). This activation approach from the vapor phase was demonstrated to be useful in a previous publication related to the preparation of UZAR-S12, a ZIF-type material [35]. In addition, this procedure minimizes possible detachment of ZIF crystals from the QCM substrates. Activated

ZIF-coated QCMs were used for measuring CO_2 adsorption. The systems prepared were named ZIF/QCM_xL, where x= 2-3-4 indicates the number of ZIF dip-coatings carried out on the QCM support.

2.6 Characterization

Different ZIF films, previously coated with Pt, were observed by scanning electron microscopy (SEM) using an Inspect-F (FEI) microscope operated at 15 kV with spatial resolution of ca. 2-3 μm. EDX experiments were conducted to detect the presence of metals from the ZIFs. Particle size distributions were obtained using ImageJ 1.50i software by counting at least 250 particles in every sample. To construct the histogram of the particle sizes, the Sturges method was used [39]. To facilitate the calculation of the ZIF coating area on the glass or QCM substrates, a specific code for reading and processing SEM images was designed in MATLAB software [40]. The standard deviations of % coating area correspond to an average from 3-4 different SEM images obtained for every sample. Powder X-ray diffraction of the ZIF (XRD) was performed at room temperature on a D-Max Rigaku diffractometer with a copper anode and a graphite monochromator to select the Cu Kα1 (λ = 0.15406 nm) radiation. The data were collected in the range 2θ = 2.5-40° and the scan speed was $0.01° \cdot s^{-1}$. Thermogravimetric analyses (TGA) of the ZIFs were performed on a Mettler Toledo TGA/SDTA 851e. Samples (10 mg) placed in 70 μL alumina pans were heated in an air flow from 25 to 900 ºC at a heating rate of $10\ ºC \cdot min^{-1}$. Nitrogen adsorption-desorption measurements were carried out at 77 K with a Micrometrics Tristar 3000 porosity analyzer. The Brunauer-Emmett-Teller (BET) method was used to calculate the specific surface areas of the ZIFs. The samples were degassed at 200 °C for 8 h. CO_2 isotherms of powdered materials were obtained at 25 ºC using a Micromeritics Surface Area and

Porosity (ASAP) 2020 analyzer. Samples were previously degassed at 200 ºC for 8 h. FTIR–ATR (Fourier transform infrared spectroscopy attenuated total reflection) spectra were collected in a Bruker Vertex 70 Spectrophotometer with a deuterated triglycine sulfate (DTGS) detector and diamond ATR Golden Gate. The wavenumber range measured in every case was between 500 and 4500 cm^{-1} with a resolution of 2 cm^{-1}. This technique was used to study the identification of functional groups on the glass surface. The contact angles of ZIF/glass samples were measured with Krüss DSA 10 MK2 equipment by dropping water drops on different places of each sample.

2.7 QCM system for gas adsorption

The QCM-based setup used in this study was previously reported by Benito et al. [20]. Fig. S1 shows a scheme of the QCM-based device. Two identical crystals of a resonant frequency of 9 MHz were placed inside a 200 mL stainless steel chamber with a custom designed QCM holder. One crystal was coated with the material to be studied, while the other was uncoated and acted as the reference. The holders were connected to an Inficon RQCM system with phase lock oscillators ranging between 5.1 and 10 MHz. The pressure inside the chamber was monitored by means of a pressure sensor. The temperature inside the chamber was controlled by two sensors and adjusted by two electric resistors. CO_2 and He flows were controlled separately by two Alicat Scientific MC-100SCCM-D/5 M mass-flow controllers. Before measuring a CO_2 adsorption isotherm, each sample was activated in the QCM chamber at 80 ºC for 1 h with a constant flow of 50 mL (STP)$\cdot min^{-1}$ of He. Then, the device was cooled down to 30 ºC maintaining the He flow until stable frequencies of both QCM crystals were reached. All the isotherms were determined at 30 ºC by using 5 different partial pressures of CO_2 in the mixture (20%, 40%, 60%, 80%, and 100% in volume) maintaining a total gas

flow of 50 mL (STP)·min^{-1}. The resonance frequency of the crystals was allowed to stabilize before changing the composition of the gas mixture for 20-40 min. A pure He flow was used for monitoring the CO_2 desorption from the ZIF/QCM. The change of resonant frequency was related to the mass of ZIFs deposited onto a QCM crystal using the Sauerbrey equation [41]: $\Delta f = -C_f \cdot \Delta m$, where Δm is the change in mass per unit area. Δf is the frequency change in Hz, C_f the sensitivity factor of the QCM crystal (0.1834 Hz·ng^{-1}·cm^2) provided by Inficon and Δf is the frequency change. This equation was also used to calculate the amount of CO_2 adsorbed by a given ZIF/QCM system.

Although the Inficon RQCM system used cannot measure the dissipation factor, the methodology followed to prepare ZIF films (dip-coating in methanol, not in aqueous media), the relatively rigid nature of ZIF nanoparticles (compared to soft polymers/biomolecules) and the exposure of ZIF films to DCM before ZIF mass determination reasonably guarantees that the assumptions made in the Sauerbrey equation can be used in this study [42].

3. Results and Discussion

3.1 ZIFs characterization

Table 1. Selected properties of ZIF-8, ZIF-67, ZIF-7, ZIF-93

ZIF crystals					ZIF films	
					CO_2 adsorbed (mmol·g^{-1})	
ZIF	**Average size (nm)**	**S_{BET} (m^2·g^{-1})**	**Vp[a] (cm^3·g^{-1})**	**Pore diameter (nm)**	**Conventional method (25 °C)**	**QCM (30 °C)**
ZIF-8	65 ±20	1536	0.64	0.34[43]	0.73	0.63
ZIF-67	285±96	1574	0.73	0.34[43]	0.70	0.60
ZIF-7	61±20	179	0.26	0.30[44]	1.80	1.23

ZIF-93	72±21	810	0.59	0.36[45]	1.60	1.24

[a]P/P_0= 0.97

The crystalline structures of ZIFs were confirmed by X-ray diffraction upon comparison with the corresponding simulated patterns (see Fig. 1). The corresponding CIF files were used to obtain the simulated patterns [7, 18, 46, 47]. The thermal stabilities of ZIFs were determined by TGA (see Fig. S2). The adsorption/desorption isotherms exhibited the expected rapid increase of nitrogen adsorption at very low relative pressure and a nearly constant adsorption at high relative pressure, in agreement with the type I isotherms expected from the ZIF microporous structures (see Fig. S3). The BET specific surface area and pore volume values were in agreement with previous reported values (see Table 1) [10], even it is true that ZIF-7 can exhibit different adsorption parameters depending on its activation conditions and due to the breathing phenomenon [18, 48]. It is well known that nitrogen (kinetic diameter of 0.36 nm) adsorption isotherms are caused by structural changes of ZIFs. In particular, the enlargement of the window size of ZIF-8 (0.34 nm) that connect its large cavities (1.16 nm) provokes the faster diffusivity of molecules through its porosity [45].

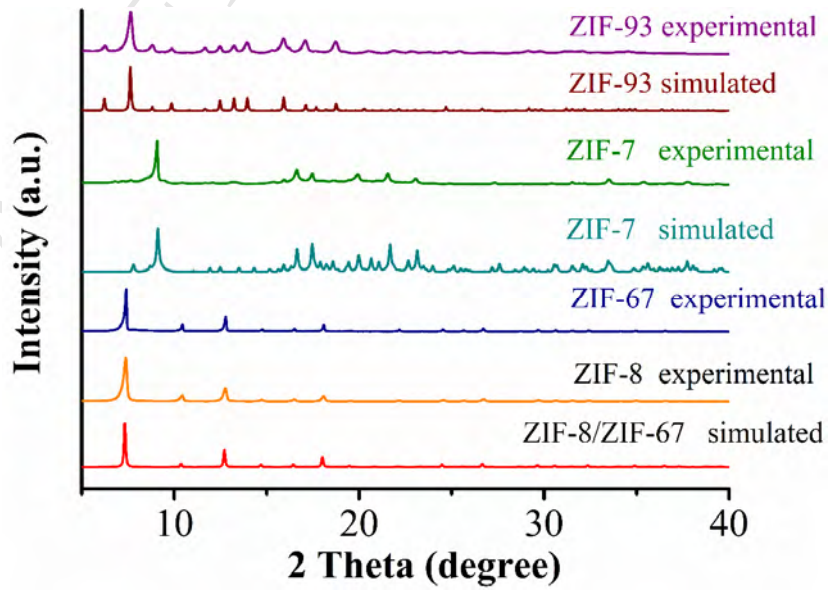

Figure 1. XRD patterns of the different zeolitic imidazolate frameworks studied in this work. The simulated patterns were obtained from the corresponding CIF files in [7, 18, 46, 47].

3.2 Characterization of ZIF/ Films

Fig. 2 shows the SEM images of homogeneous ZIF-8, ZIF-67, ZIF-7 and ZIF-93 thin films (1L and 2L) deposited by dip-coating onto glass substrates. ZIFs/glass_2L presents the best coverage among all the studied samples. Fig. S4 shows the SEM images used to calculate the percentages of coated area of the different ZIF containing samples (see Table 2) and the average particle sizes of the corresponding crystals: 65±19, 285±96, 61±20 and 72± 21 nm for ZIF-8, ZIF-67, ZIF-7 and ZIF-93, respectively (see Table 1 and Fig. S5). ZIF/glass_2L samples were obtained after depositing a second layer of the respective ZIF by dip coating on top of a ZIF/glass_1L sample. In all cases, the second coating increased the percentage of surface coverage. For the ZIF-8/glass_2L, ZIF-67/glass_2L, ZIF-7/glass_2L and ZIF-93/glass_2L films, the coated area coverages are 99.8±0.2%, 99.1±0.3%, 99.1±0.2% and 99.9±0.1%, respectively. These results suggest that the voids generated during the first layer deposition were filled during the second one. Interestingly, Fig. 3 shows that the coating areas of the ZIFs/QCM_2L are similar to those of the ZIFs/glass_2L samples, indicating that the procedure developed on glass supports was fully transferred to QCM substrates (see also Table 2). The importance of the functionalization of glass is evidenced in ZIF-8 and ZIF-67 coating tests when they were carried out on non-functionalized glass (Fig. S6), where an incomplete coating of ZIF was only achieved. Moreover, as an example related to ZIF-93 on glass, Fig. S7 shows ca. 6 mm^2 and ca. 0.0001 mm^2 coating areas

(coming from different SEM magnifications) highlighting the general homogeneity of the ZIF films.

The tuning of the coating thickness and homogeneity is depending not only on the adjustment of the withdrawal speed but also on the concentration and solvent of the dispersion as already mentioned (see sections 2.4 and 2.5). Methanol was used here because of its easy availability and low surface tension (22.1 mN/m). Moreover, methanol is as volatile as to promote relatively fast evaporation, what helps prevent dewetting. All this is necessary to obtain homogeneous films [30]. Additionally, EDX mapping in Fig. S8 of ZIF/glass_2L also shows a homogeneous distribution of Zn and Co contents, corroborating that the ZIFs are evenly distributed on the substrates. Since in these images ZIF particle sizes are far below the spatial resolution of the technique (ca. 2-3 μm), the color spots should correspond to metal coming from several ZIF particles.

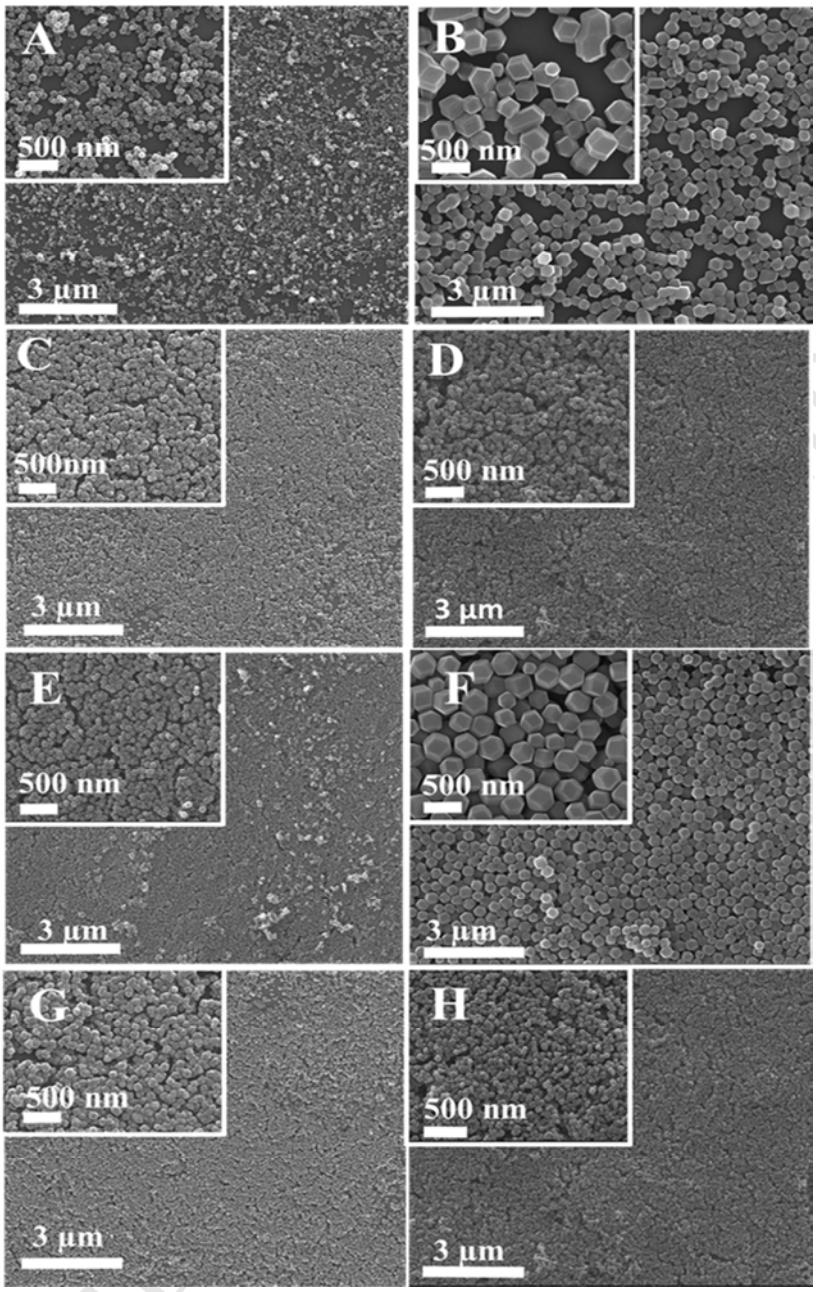

Figure 2. SEM images of ZIFs on glass substrates: (A) ZIF-8/glass_1L; (B) ZIF-67/glass _1L; (C) ZIF-93/glass_1L; (D) ZIF-7/glass_1L; (E) ZIF-8/glass_2L; (F) ZIF-67/glass_1L; (G) ZIF-93/glass_2L; (H) ZIF-7/glass_2L.

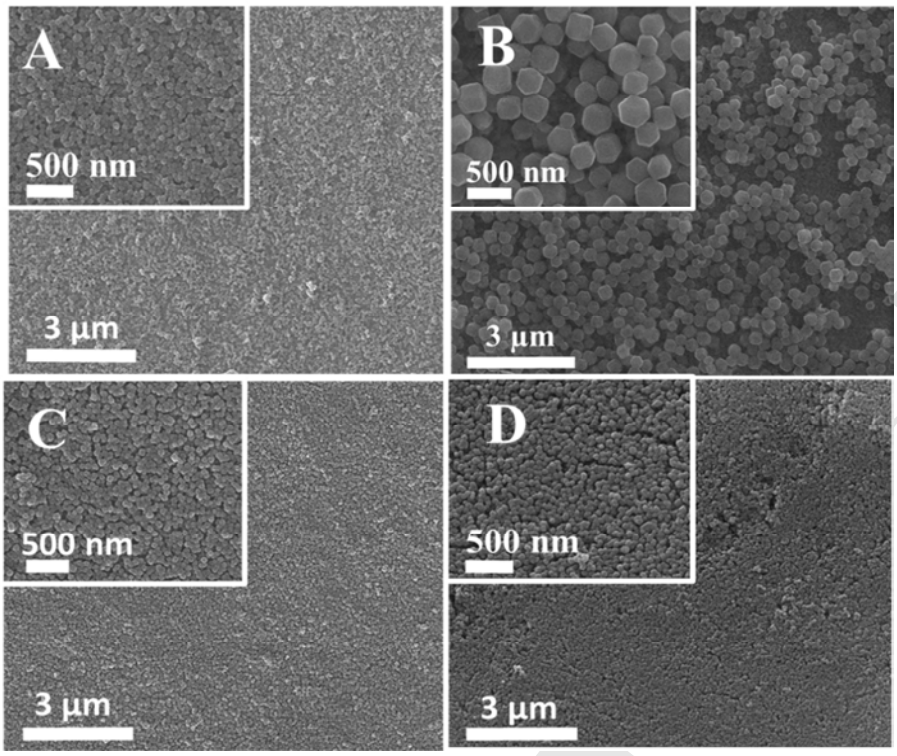

Figure 3. SEM images of ZIF/QCM_2L: (A) ZIF-8; (B) ZIF-67; (C) ZIF-93; and (D) ZIF-7.

The SEM cross-section images provided in Fig. S9 for films ZIF-8/glass_3L and ZIF-93/glass_3L allow one to check that the number of dip coating depositions is, particularly for ZIF-8, directly related to the total thickness of the ZIF layer. Thus, three coatings of ZIF-8, with average particle size of ca. 65 nm (see Fig. S5), produced an average thickness of 178±33 nm. This agrees with the fact that the current technique allows a control of the ZIF thickness by running successive dip coatings, even though the SEM cross sections are not good enough to demonstrate the coating homogeneity as the top images of the samples (Figs. 2 and 3).

Figs. 4A and B show the ATR-FTIR spectra of the surfaces of ZIFs/glass_3L samples (three coatings were used this time to enhance the accuracy of the measurement) constituted by crystals of ZIF-8, ZIF-67, ZIF-7 and ZIF-93. The peaks that emerge at 880 cm^{-1} and 1249 cm^{-1} are allocated to Si–OH stretching and Si–O

bonds, respectively [49, 50]. In Fig. 4A new bands of 1606 to 690 cm^{-1} are observed in samples with ZIF-8 and ZIF-67 (1606 and 1580 cm^{-1} corresponding to C=C and C-N, respectively). Fig. 4B also shows specifically in sample ZIF-93/glass_3L the bands at1633 and 1658 cm^{-1} characteristic of the aldehyde group CHO of ZIF-93. The absorption band at 740 cm^{-1} in the ZIF-7 spectrum is associated with the typical out-of-plane C–H bending vibration of ortho-disubstituted benzene from the bIm ligand [51]. Additionally, the multi-peaks between 1538 and 650 cm^{-1} of ZIF-7/glass_3L and ZIF-93 /glass_3L spectra are consistent with the presence of ZIF nanocrystals on the substrates.

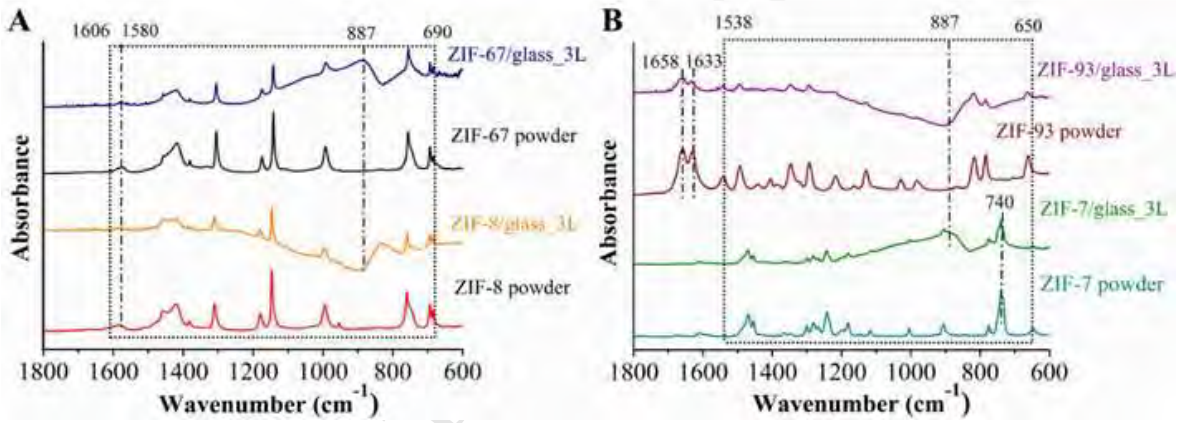

Figure 4. ATR-FTIR spectra of: (A) ZIF-8/glass_3L (with background subtraction), ZIF-67/glass_3L and ZIF-8 and ZIF-67 powders; (B) ZIF-7/glass_3L, ZIF-93/glass_3L (with background subtraction) and ZIF-7 and ZIF-93 powders.

To study the properties of the films in terms of hydrophilicity/hydrophobicity, the contact angles of the cover glass, QCM, and ZIF films were measured for 1, 3 and 4 coated samples to show clear tendencies of this parameter with the number of coatings (see Table 2 where after only 2 coatings the coating area parameter was >99%). The glass support showed a contact angle of 60±3º. After piranha cleaning, this contact

angle decreased to 24º due to the formation of hydroxyl groups after the surface oxidation and the eventual removal of any organic impurity. After the treatment with PEG silane, the contact angle increased to 47±0º due to the presence of hydrophobic groups on the surface [52]. When a ZIF was deposited onto PEG modified glass support, the contact angle increased even more (see Table 2). This is due to the presence of the ZIF layer on the support, which enhances the hydrophobicity of the surface due to the presence of the imizadolate type linkers of ZIFs. The surface of a new, untreated QCM is more hydrophobic with a contact angle of 84±1º. After cleaning, this value decreased to 78±0º. The functionalization process led to an increase of this value to 90±2º due to the presence of hydrophobic groups on the surface. In the same way, when a ZIF layer was added and then exposed to dichloromethane vapor for its activation on the surface of QCM, it became more hydrophobic. Thus ZIF-8/QCM and ZIF-7/QCM show contact angles of 122±0º and 137±2º, respectively, greatly exceeding 90º owing to the hydrophobic character of the ZIF materials that totally coated the corresponding QCM surface. This did not occur with sample ZIF-67/QCM (74±5º), due probably to its larger particle size crystals, or ZIF-93/QCM (75±1º), because this ZIF is relatively hydrophilic due to the aldehyde group CHO. QCM samples showed larger contact angles than glass samples, what is due to the organic functionalization with MEO-PEG-SH of the former. It should be noted that these contact angle measurements can also be affected by the roughness of the surface due to the entrapment of air bubbles between the substantially rough surface and the drop of water [53].

Table 2. Coating areas and contact angles of films

	Coating area (%)			**Contact angle (°)**		
ZIF	**ZIF/glass_1L**	**ZIF/glass_2L**	**ZIF/QCM_2L**	**ZIF/glass_1L**	**ZIF/glass_3L**	**ZIF/QCM_4L**
ZIF-8	83.6±0.5	99.8±0.2	99.8±0.3	62±2	78±5	122±0
ZIF-67	94.0±1.0	99.1±0.3	99.7±0.4	60±5	69±1	74 ±5

ZIF-7	98.9±0.6	99.1±0.2	99.4±0.2	96±4	109±5	137±2
ZIF-93	99.8±0.6	99.9±0.1	99.9±0.2	52±5	67±4	75±1

The XRD patterns of as-prepared ZIF/films are shown in Fig. 5. They demonstrate that the fabrication of these ZIF structures on the substrates was carried out without affecting the crystallinity of the ZIFs and without the presence of impure phases. However, only some XRD peaks corresponding to the highest intensities of ZIFs can be observed due to the small amount of ZIF crystals present in the thin ZIF layers deposited on the glass substrates. In any event, no preferential crystallographic orientation can be claimed.

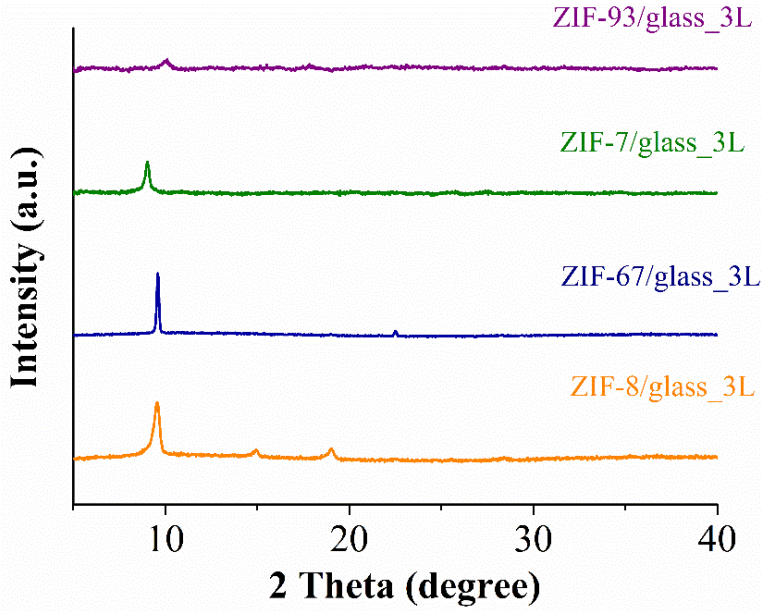

Figure 5. XRD patterns of ZIF/glass_3L samples with ZIF-8, ZIF-67, ZIF-7 and ZIF-93.

3.3 CO_2 adsorption studies using ZIF/QCMs

Different methods of activation were carried out on ZIF-8/QCM (see Fig. S10). The goal was to find the most suitable activation method in which conventional powder and QCM CO_2 adsorption capacities were as close as possible: i) degassing at 65 ºC in

an oven; ii) contact with methanol vapor for 12 h; or iii) exposure to DCM vapor for 12 h. The CO_2 adsorption studies were performed with the QCM-based setup at 80 ºC and pressure values up to 100 kPa following the procedure described in section 2.7. The last two procedures involve exchanging water (mostly in the case of hydrophilic ZIF-93) and DMF (in the case of ZIF-7) molecules for highly volatile organic vapors more easily removed by simple thermal heating at the limiting temperature operating in the QCM rig (80 ºC, due to the limited thermal resistance of the electronic components). In addition, the samples saturated with either DCM or methanol are less easily polluted during their handling before being coupled in the QCM holder. As a result, CO_2 adsorption values at 100 kPa of 0.57, 0.59 and 0.63 $mmol \cdot g^{-1}$ were obtained for activation procedures 1, 2 and 3, respectively, comparable to that of the ZIF-8 powder (0.73 $mmol \cdot g^{-1}$).

Fig. 6 shows the experimental CO_2 adsorption isotherms at 30 °C of ZIF-8/QCM_4L, ZIF-67/QCM_4L, ZIF-7/QCM_4L, and ZIF-93/QCM_4L (four coatings were used to obtain more reliable results) compared with powder isotherms of ZIF nanoparticles as determined by the conventional analytical method. Note that QCM experiments (see Fig. S11 for the frequency-time curves produced from the different ZIF/QCMs) are performed with small sample quantities of just a few micrograms, allowing heat and mass transfer issues that occur with larger sample sizes to be avoided [54]. In fact, the amount of adsorbent mass of ZIFs films deposited on QCM substrates was in the 7-10 μg range, i.e. a few micrograms versus ca. 100 mg used in the conventional adsorption method. The conventional and QCM adsorption methods present similar CO_2 isotherm shapes and CO_2 adsorption capacities not so far apart (see Table 1), bearing in mind that the thermal treatment in the QCM is limited to 80 ºC, a temperature not as efficient as that used for the activation in conventional powder

adsorption (200 ºC). In consequence, ZIF/QCMs with ZIF-8, ZIF-67, ZIF-7 and ZIF-93 achieved 15%, 5%, 31% and 23%, respectively, lower CO_2 adsorption capacities than with the conventional method. The conventional powder adsorption results are in agreement with previous experimental results [18, 43, 55].

The good CO_2 adsorption results achieved were favored by the activation method based on exchange with dichloromethane vapor. This is a solvent that can access the porous structure of the ZIFs (kinetic diameter 0.33 nm and dielectric constant = 9.1) [48]. This methodology provided the expected types of isotherms (particularly in the cases of ZIF-7 and ZIF-93, where a saturating behavior is suggested at the working pressure conditions, see Figs. 6C and D) that demonstrate the microporosity of the ZIFs (see Table 1) for an easier accessibility and faster diffusion rate of CO_2 molecules (kinetic diameter 0.33 nm) [56]. The different adsorption capacities can be related to the ZIF composition. CO_2 is a non-polar molecule with no dipole moment, but with significant interaction with hydrophilic and polar surfaces due to its two dipoles [43]. Therefore, this molecule is attracted by highly charged polar groups such as hydroxyl or oxygenated or amine substituents. In this sense, ZIF-8 and ZIF-67 have an absence of strong nucleophile groups which justifies their low CO_2 adsorptions observed [7].The frequency changes of ZIF-8 and ZIF-67 were linear as a function of pressure, as were the CO_2 amounts adsorbed (Figs. 6A and B).

Due to their framework flexibility, ZIFs can undergo structural transformations during the sorption process [57] due to temperature [43, 58, 59] and pressure changes [60]. Among ZIFs, ZIF-8 is the most widely investigated. ZIF-8 exhibits the so-called gate-opening phenomenon and also a certain structural expansion [61, 62]. ZIF-7 undergoes a phase-to-phase transformation upon guest adsorption–desorption [46]. In consequence, ZIF-7/QCM exhibits an S-shape isotherm (see Fig. 6C) in agreement with

previous results described in the literature, where this adsorption isotherm is associated with a transition of phase II (empty pore) to phase I (guest-loaded) [62, 63]. However, the amount of gas adsorbed does not reach the values reported due to the strong thermal treatment needed for its complete activation [62, 63] and the difficulty of completely removing the solvent (DMF) from its inner cavities [18, 48]. In ZIF-93/QCM film, which is more hydrophilic than the others, the carbonyl groups present in the ligands of ZIF-93 allow the formation of hydrogen bonds, thus enabling a stronger adsorption at low pressure. Fig. S11 shows the effect of sweeping with He at the end of the adsorption experiment. The resonant frequencies recovered almost completely (87-93%) their initial values, indicating an almost reversible process.

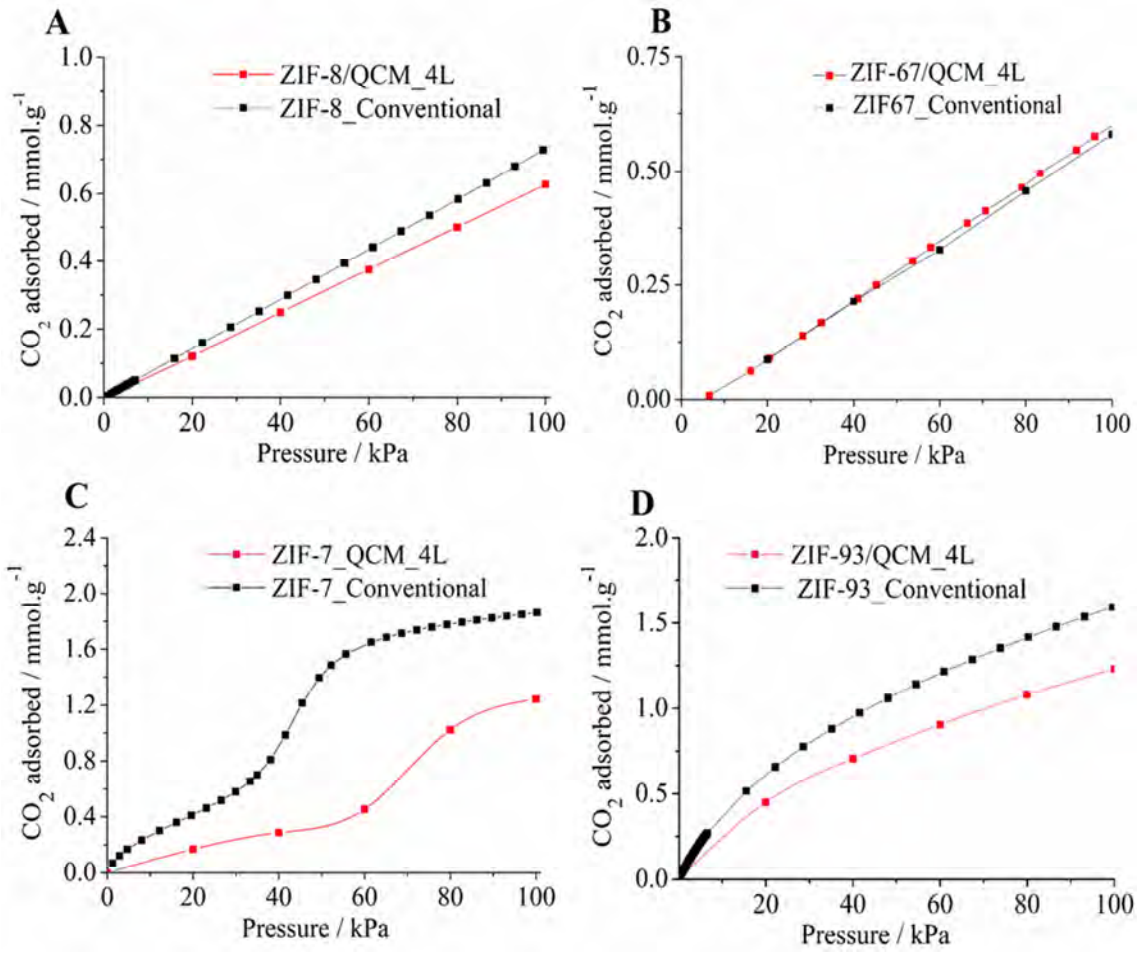

Figure 6. CO_2 adsorption isotherms achieved by conventional (25 ºC) and QCM (30 ºC) methods for: (A) ZIF-8, (B) ZIF-67, (C) ZIF-7 and (D) ZIF-93.

The results obtained demonstrate that it is possible to obtain thin films with extremely high coverages (99.4%-99.9% after two coatings) with four different MOFs by using a simple dip-coating technique. When the coatings were implemented on QCM substrates, the ZIF/QCMs obtained gave rise to similar CO_2 adsorption values to those obtained from fully activated powders for the ZIFs under study. Another important advantage of this method is its simplicity compared with others requiring stepwise depositions of MOFs on SAM (self-assembled monolayer) surfaces, for achieving crystalline, phase-pure, densely packed (even though the shape of crystals can be distinguished in the current work), and oriented SURMOFs (MOFs attached to a surface) [64]. Besides, after the availability of the MOF nanoparticles (what may take additional time as described in the experimental section), the times needed to fabricate ZIF/QCM_1L and ZIF/QCM_4L are 14 min and 56 min, respectively, shorter or comparable to other common methods. For example, Langmuir-Blodgett films of MIL-101(Cr) needed 3 h to be prepared [20], and the fabrication of a MOF-5 film using the liquid phase epitaxial method required 72 h [65]. ZIF-8 coatings were obtained by microwave-assisted solvothermal synthesis for 1 h on Si and SiO_2 substrates previously modified by atomic layer deposition of ZnO [66]. The spray method can give rise to uniform and homogeneous coatings of MOFs (SURMOFs), where isolated crystals were not distinguishable, in 30 min, with 20 deposition cycles [25]. Chemical vapor deposition of ZIF-8 was performed on a ZnO coated substrate in three steps with a total duration of 40 min [67]. In this work, the minimum number of layers deposited to obtain good ZIF films is four, far below that of others methods as the layer-by-layer

epitaxial growth, where need up to 80 layers were necessary to obtain suitable films of HKUST-1 [68].

4. Conclusions

A dip-coating method carried out at room temperature has been shown to be a simple and efficient procedure to coat different ZIFs (ZIF-8, ZIF- 67, ZIF-7 and ZIF-93) on glass and QCM type substrates. Using this method, ZIF homogeneous thin films were obtained with a controlled number of nanoparticle monolayers and maintaining the crystallinity of the as prepared ZIFs. The activation of the films was facilitated by using dichloromethane vapors. This allowed the achievement of CO_2 adsorption isotherms of the same type as those obtained with activated powders at 200 ºC but giving rise to somewhat lower adsorption capacities, depending on the nature and pore size of the ZIFs. ZIF-8 and ZIF-67 presented values similar to those of their respective powders; however, the differences were larger than 20% for ZIF-7 and ZIF-93.

Acknowledgements

Financial support from the Spanish Ministry of Economy and Competitiveness and FEDER (MAT2016-77290-R), the European Social Fund and the Aragón Government (DGA, T05) is gratefully acknowledged. L.S. is also grateful for a Ph.D. grant from Becas Santander Universidades. The microscopy work was carried out in the Laboratorio de Microscopías Avanzadas at the Instituto de Nanociencia de Aragón (LMA-INA, Universidad de Zaragoza). The use of the Servicio General de Apoyo a la Investigación-SAI (Universidad de Zaragoza) is also acknowledged.

References

[1] K.S. Park, Z. Ni, A.P. Côté, J.Y. Choi, R. Huang, F.J. Uribe-Romo, H.K. Chae, M. O'Keeffe, O.M. Yaghi, Proc. Natl. Aca. Sci. USA 103 (2006)) 10186-10191.
[2] X.-C. Huang, Y.-Y. Lin, J.-P. Zhang, X.-M. Chen, Angew. Chem. Int. Ed. 118 (2006) 1587-1589.
[3] A. Phan, C.J. Doonan, F.J. Uribe-Romo, C.B. Knobler, M. O'Keeffe, O.M. Yaghi, Synthesis, Acc. Chem. Res., 43 (2010) 58-67.
[4] H.-L. Jiang, B. Liu, T. Akita, M. Haruta, H. Sakurai, Q. Xu, J. Am. Chem. Soc. 131 (2009) 11302-11303.
[5] S. Diring, D.O. Wang, C. Kim, M. Kondo, Y. Chen, S. Kitagawa, K.-i. Kamei, S. Furukawa, Nat. Commun.4 (2013) 2684.
[6] I. Erucar, S. Keskin, Ind. Eng. Chem. Res., 55 (2016) 1929–1939.
[7] R. Banerjee, A. Phan, B. Wang, C. Knobler, H. Furukawa, M. O'Keeffe, O.M. Yaghi, Science. 319 (2008) 939-943.
[8] B. Zornoza, B. Seoane, J.M. Zamaro, C. Tellez, J. Coronas, ChemPhysChem, 12 (2011) 2781-2785.
[9] J. van den Bergh, C. Gücüyener, E.A. Pidko, E.J.M. Hensen, J. Gascon, F. Kapteijn, Chem. A Eur. J. 17 (2011) 8832-8840.
[10] L. Sarango, L. Paseta, M. Navarro, B. Zornoza, J. Coronas, J. Ind. Eng. Chem. 59 (2018) 8-16.
[11] J.B. DeCoste, G.W. Peterson, Chem. Rev. 114 (2014) 5695-5727.
[12] D. Liu, K. Lu, C. Poon, W. Lin, Inorg. Chem. 53 (2014) 1916-1924.
[13] Y. Hwang, H. Sohn, A. Phan, O.M. Yaghi, R.N. Candler, Nano Lett., 13 (2013) 5271-5276.
[14] S. Liu, Z. Xiang, Z. Hu, X. Zheng, D. Cao, J. Mater. Chem, 21 (2011) 6649-6653.
[15] G. Lu, J.T. Hupp, J. Mater. Chem, 132 (2010) 7832-7833.
[16] M. Tu, S. Wannapaiboon, K. Khaletskaya, R.A. Fischer, Adv. Funct. Mater. 25 (2015) 4470-4479.
[17] X. Huang, J. Zhang, X. Chen, Chinese Sci. Bull. 48 (2003) 1531-1534.
[18] W. Morris, N. He, K.G. Ray, P. Klonowski, H. Furukawa, I.N. Daniels, Y.A. Houndonougbo, M. Asta, O.M. Yaghi, B.B. Laird, J. Phys. Chem. 116 (2012) 24084-24090.
[19] O. Shekhah, M. Eddaoudi, Chem. Commun., 49 (2013) 10079-10081.
[20] J. Benito, S. Sorribas, I. Lucas, J. Coronas, I. Gascon, ACS Appl. Mater. Interfaces, 8 (2016) 16486-16492.
[21] I. Stassen, M. Styles, G. Grenci, Hans V. Gorp, W. Vanderlinden, Steven D. Feyter, P. Falcaro, D.D. Vos, P. Vereecken, R. Ameloot, Nat. Mater. 15 (2015) 304.
[22] D.-Y. Kim, B.N. Joshi, J.-G. Lee, J.-H. Lee, J.S. Lee, Y.K. Hwang, J.-S. Chang, S. Al-Deyab, J.-C. Tan, S.S. Yoon, Chem. Eng. J. 295 (2016) 49-56.
[23] H.K. Arslan, O. Shekhah, J. Wohlgemuth, M. Franzreb, R.A. Fischer, C. Wöll, Adv. Funct. Mater., 21 (2011) 4228-4231.
[24] S. Hermes, M.K. Schröter, R. Schmid, L. Khodeir, M. Muhler, A. Tissler, R.W. Fischer, R.A. Fischer, Angew. Chem. Int. Ed. 44 (2005) 6237-6241.
[25] R. Ameloot, L. Stappers, J. Fransaer, L. Alaerts, B.F. Sels, D.E. De Vos, Chem. Mater. 21 (2009) 2580-2582.
[26] P. Horcajada, C. Serre, D. Grosso, C. Boissière, S. Perruchas, C. Sanchez, G. Férey, Adv. Mater. 21 (2009) 1931-1935.
[27] O. Dalstein, E. Gkaniatsou, C. Sicard, O. Sel, H. Perrot, C. Serre, C. Boissière, M. Faustini, Angew. Chem. 129 (2017) 14199-14203.
[28] D. Grosso, J. Mater. Chem. 21 (2011) 17033-17038.
[29] M. Faustini, C. Boissière, L. Nicole, D. Grosso, Chem. Mater. 26 (2014) 709-723.

[30] M. Faustini, B. Louis, P.A. Albouy, M. Kuemmel, D. Grosso, J. Phys. Chem. 114 (2010) 7637-7645.
[31] M. Benz, L. Benz, S.V. Patel, Anal. Chem. 87 (2015) 2779-2787.
[32] E. Biemmi, A. Darga, N. Stock, T. Bein, Microporous Mesoporous Mater. 114 (2008) 380-386.
[33] Z. Ihdene, A. Mekki, B. Mettai, R. Mahmoud, B. Hamada, M.M. Chehimi, Sens. Actuator B-Chem. 203 (2014) 647-654.
[34] M. Tu, R.A. Fischer, J. Mater. Chem. A, 2 (2014) 2018-2022.
[35] A. Perea-Cachero, B. Seoane, B. Diosdado, C. Tellez, J. Coronas, RSC Adv. 6 (2016) 260-268.
[36] J. Cravillon, S. Münzer, S.-J. Lohmeier, A. Feldhoff, K. Huber, M. Wiebcke, Chem. Mater. 21 (2009) 1410-1412.
[37] X. Liu, Y. Li, Y. Ban, Y. Peng, H. Jin, H. Bux, L. Xu, J. Caro, W. Yang, Chem. Commun., 49 (2013) 9140-9142.
[38] T. Yang, Y. Xiao, T.-S. Chung, Energy Environ. Sci. 4 (2011) 4171-4180.
[39] F.H. Aragón, P.E.N. de Souza, J.A.H. Coaquira, P. Hidalgo, D. Gouvêa, Physica B Physica B: Condensed Matter. 407 (2012) 2601-2605.
[40] M.S. Nixon, A.S. Aguado, Chapter 3 - Basic image processing operations, in: Feature Extraction & Image Processing for Computer Vision (Third edition), Academic Press, Oxford, 2012, pp. 83-136.
[41] A. Venkatasubramanian, M. Navaei, K.R. Bagnall, K.C. McCarley, S. Nair, P.J. Hesketh, J. Phys. Chem. 116 (2012) 15313-15321.
[42] Q. Chen, S. Xu, Q. Liu, J. Masliyah, Z. Xu, Adv. Colloid Interface Sci., 233 (2016) 94-114.
[43] F. Cacho-Bailo, I. Matito-Martos, J. Perez-Carbajo, M. Etxeberría-Benavides, O. Karvan, V. Sebastián, S. Calero, C. Téllez, J. Coronas, Chem. Sci. 8 (2017) 325-333.
[44] Y.S. Li, F.Y. Liang, H. Bux, A. Feldhoff, W.S. Yang, J. Caro, Angew. Chem. Int. Ed. 122 (2010) 558-561.
[45] K.G. Ray, D.L. Olmsted, J.M.R. Burton, Y. Houndonougbo, B.B. Laird, M. Asta, Chem. Mater, 26 (2014) 3976-3985.
[46] P. Zhao, G.I. Lampronti, G.O. Lloyd, M.T. Wharmby, S. Facq, A.K. Cheetham, S.A.T. Redfern, Chem. Mater, 26 (2014) 1767-1769.
[47] B.P. Biswal, T. Panda, R. Banerjee, Chem. Commun., 48 (2012) 11868-11870.
[48] C. Cuadrado-Collados, J. Fernandez-Catala, F. Fauth, Y.Q.Q. Cheng, L.L. Daemen, A.J. Ramirez-Cuesta, J. Silvestre-Albero, J. Mater. Chem. A, 5 (2017) 20938-20946.
[49] T. Rezayi, M.H. Entezari, New J. Chem. 40 (2016) 2582-2591.
[50] T. Oh, C.K. Choi, Phys. Soc. 56 (2010) 1150-1155.
[51] M. Tu, C. Wiktor, C. Rosler, R.A. Fischer, Chem. Commun. 50 (2014) 13258-13260.
[52] N. Tillman, A. Ulman, J.S. Schildkraut, T.L. Penner, J. Amer. Chem. Soc, 110 (1988) 6136-6144.
[53] D. Quéré, Physica A: Statistical Mechanics and its Applications, 313 (2002) 32-46.
[54] M. Tsotsalas, P. Hejcik, K. Sumida, Z. Kalay, S. Furukawa, S. Kitagawa, J. Amer. Chem. Soc. 135 (2013) 4608-4611.
[55] J. Xie, N. Yan, F. Liu, Z. Qu, S. Yang, P. Liu, Env. Sci. Eng. 8 (2014) 162-168.
[56] P. Chowdhury, S. Mekala, F. Dreisbach, S. Gumma, Microporous Mesoporous Mater.152 (2012) 246-252.
[57] L. Zhang, Z. Hu, J. Jiang, J. Amer. Chem. 135 (2013) 3722-3728.

[58] T.D. Bennett, D.A. Keen, J.-C. Tan, E.R. Barney, A.L. Goodwin, A.K. Cheetham, Angew. Chem. Int. Ed., 50 (2011) 3067-3071.
[59] F. Cacho-Bailo, M. Etxeberría-Benavides, O. David, C. Téllez, J. Coronas, ACS Appl. Mater. Interfaces, 9 (2017) 20787-20796.
[60] T.D. Bennett, P. Simoncic, S.A. Moggach, F. Gozzo, P. Macchi, D.A. Keen, J.-C. Tan, A.K. Cheetham, Chem. Commun., 47 (2011) 7983-7985.
[61] D. Fairen-Jimenez, R. Galvelis, A. Torrisi, A.D. Gellan, M.T. Wharmby, P.A. Wright, C. Mellot-Draznieks, T. Duren, Dalton Trans. 41 (2012) 10752-10762.
[62] S. Aguado, G. Bergeret, M.P. Titus, V. Moizan, C. Nieto-Draghi, N. Bats, D. Farrusseng, New J. Chem, 35 (2011) 546-550.
[63] Y. Du, B. Wooler, M. Nines, P. Kortunov, C.S. Paur, J. Zengel, S.C. Weston, P.I. Ravikovitch, J. Amer. Chem. Soc. 137 (2015) 13603-13611.
[64] K. Yusenko, M. Meilikhov, D. Zacher, F. Wieland, C. Sternemann, X. Stammer, T. Ladnorg, C. Wöll, R.A. Fischer, CrystEngComm, 12 (2010) 2086-2090.
[65] S. Hermes, F. Schröder, R. Chelmowski, C. Wöll, R.A. Fischer, J. Amer. Chem. Soc. 127 (2005) 13744-13745.
[66] K. Kira, T. Stuart, T. Min, W. Suttipong, S. Andreas, M. Robert, L. Alfred, V.T. Gustaaf, F.R. A., Adv. Funct. Mater., 24 (2014) 4804-4811.
[67] I. Stassen, M. Styles, G. Grenci, H. Van Gorp, W. Vanderlinden, S. De Feyter, P. Falcaro, D. De Vos, P. Vereecken, R. Ameloot, Nat. Mater. 15 (2015) 304-310.
[68] N. Nijem, K. Fürsich, S.T. Kelly, C. Swain, S.R. Leone, M.K. Gilles, Cryst. Growth Des. 15 (2015) 2948-2957.

Figure captions

Figure 1. XRD patterns of the different zeolitic imidazolate frameworks studied in this work. The simulated patterns were obtained from the corresponding CIF files in [7, 18, 46, 47].

Figure 2: SEM images of ZIFs on glass substrates: (A) ZIF-8/glass_1L; (B) ZIF-67/glass _1L; (C) ZIF-93/glass_1L; (D) ZIF-7/glass_1L; (E) ZIF-8/glass_2L; (F) ZIF-67/glass_1L; (G) ZIF-93/glass_2L; (H) ZIF-7/glass_2L.

Figure 3: SEM images of ZIF/QCM_2L using ZIF: (A) ZIF-8; (B) ZIF-67; (C) ZIF-93; and (D) ZIF-7.

Figure 4. ATR-FTIR of: (A) ZIF-8/glass_3L, ZIF-67/glass_3L and ZIF-8 and ZIF-67 powders; (B) ZIF-7/glass_3L, ZIF-93/glass_3L and ZIF-7 and ZIF-93 powders.

Figure 5. XRD pattern of ZIF/glass_3L of: ZIF-8, ZIF-67, ZIF-7/glass and ZIF-93.

Figure 6. CO_2 adsorption isotherms achieved by conventional and QCM methods for: (A) ZIF-8, (B) ZIF-67, (C) ZIF-7 and (D) ZIF-93.

- Thin films of four zeolitic-imidazolate frameworks (ZIF-8, ZIF-67, ZIF-7, and ZIF-93).
- Films fabricated by a dip-coating on glass and quartz crystal microbalance (QCM) substrates.
- ZIFs and homogeneous coatings were obtained and characterized by XRD, TGA, SEM, FTIR, contact angle and N_2 adsorption.
- CO_2 adsorption of the coatings was studied using a QCM device.

Supporting information

Homogeneous thin coatings of zeolitic imidazolate frameworks prepared on quartz crystal sensors for CO_2 adsorption

Lilian Sarango,[a,b] Javier Benito,[c] Ignacio Gascón,[c] Beatriz Zornoza,[a] and Joaquín Coronas[a,*]

[a]Chemical and Environmental Engineering Department and Instituto de Nanociencia de Aragón (INA), Universidad de Zaragoza, 50018 Zaragoza, Spain

[b]Electronics Engineering Career, Salesian Polytechnic University, Cuenca, Ecuador

[c]Departamento de Química Física, Facultad de Ciencias, and Instituto de Nanociencia de Aragón (INA), Universidad de Zaragoza, 50018 Zaragoza, Spain

*Corresponding author: coronas@unizar.es

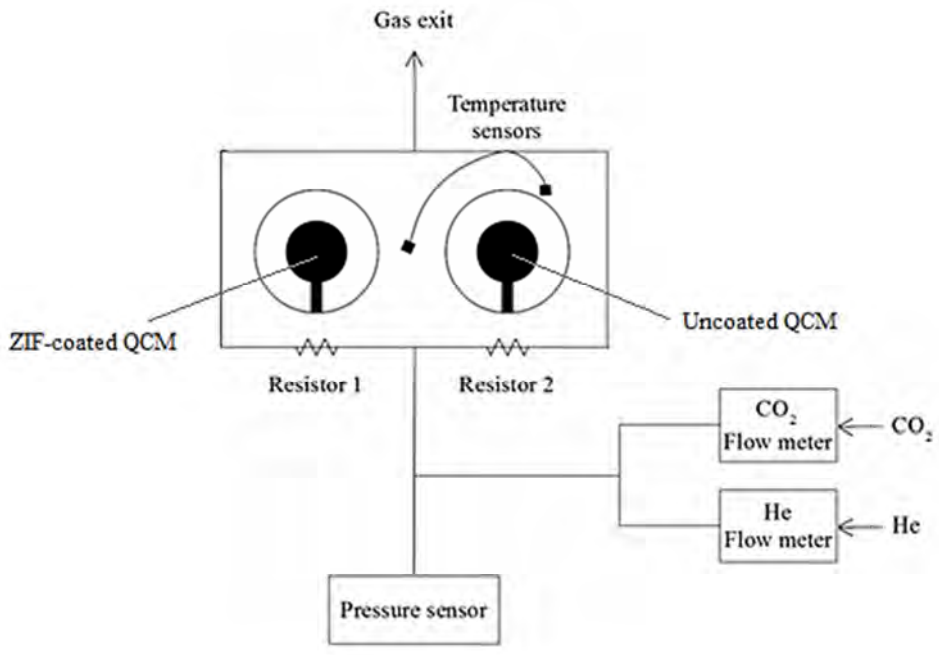

Figure S1. Scheme of the QCM-based device used in CO_2 adsorption studies.

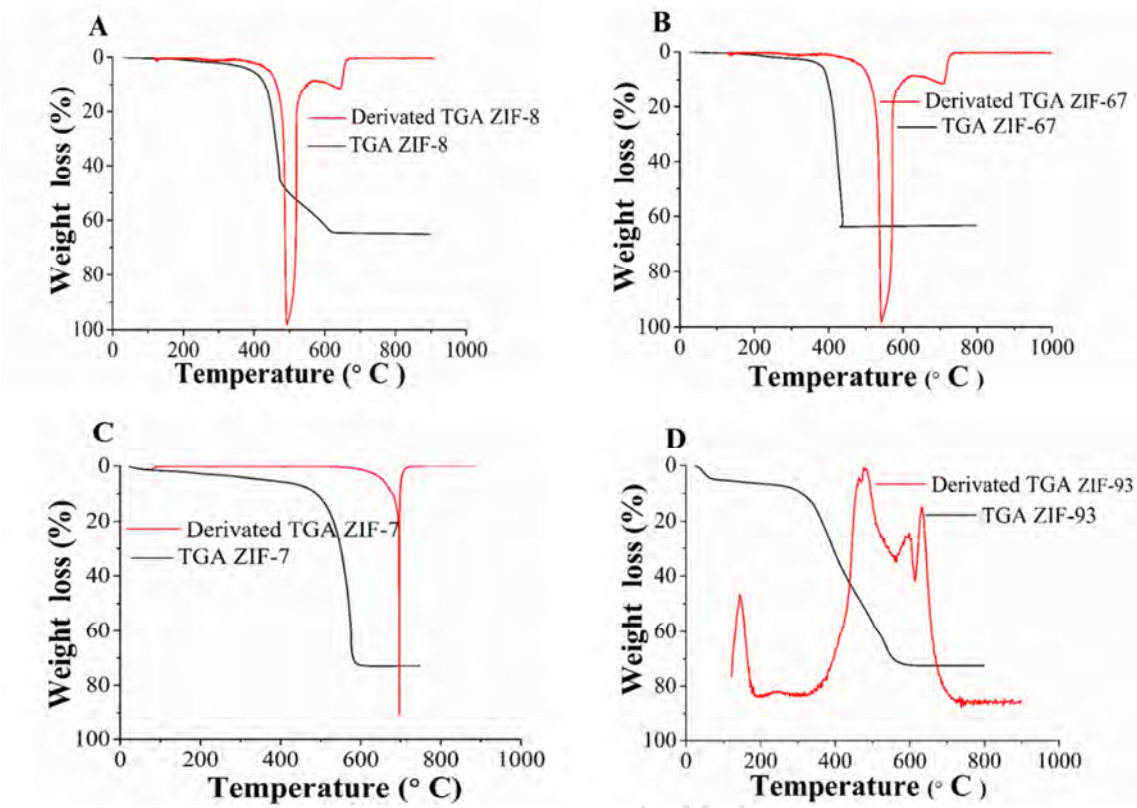

Figure S2. TGA curves of: (A) ZIF-8, (B) ZIF-67, (C) ZIF-7, and (D) ZIF-93

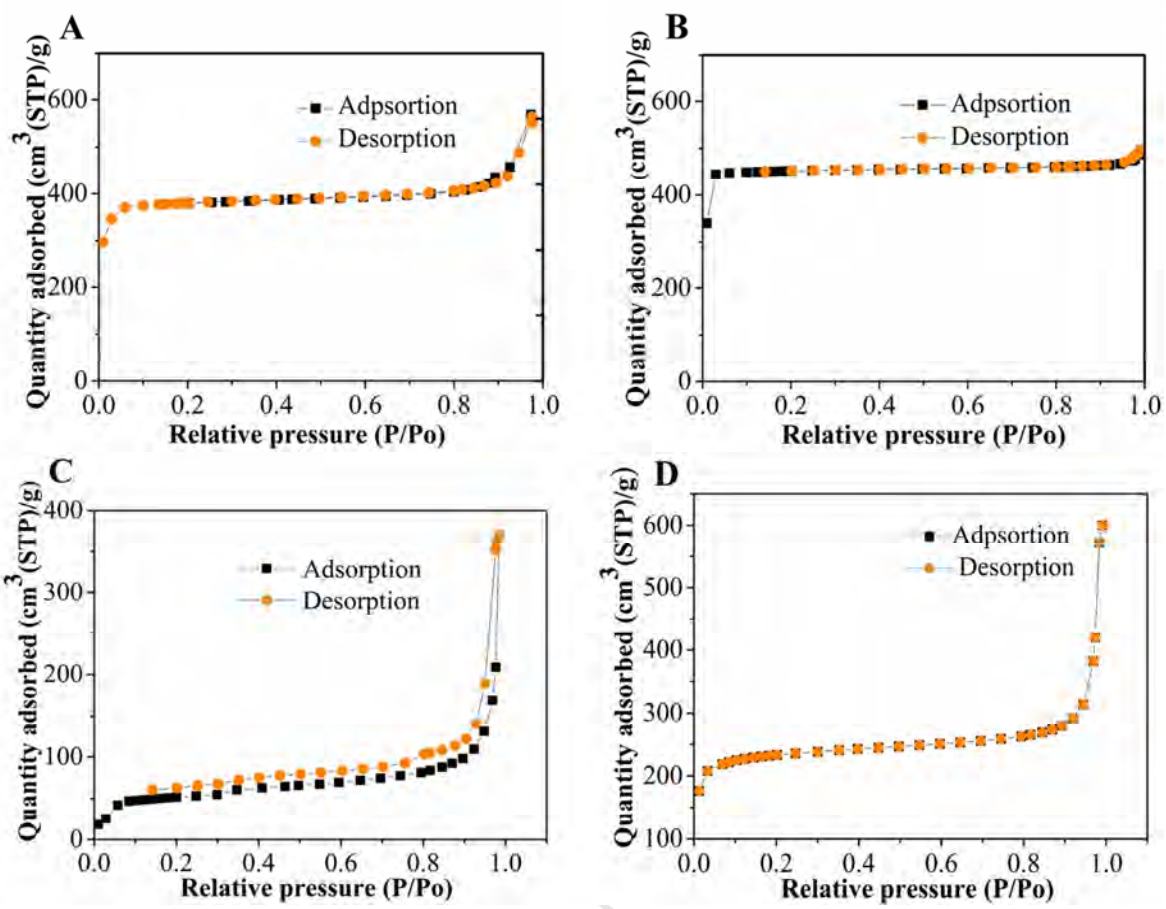

Figure S3. Nitrogen adsorption/desorption isotherms of: (A) ZIF-8, (B) ZIF-67, (C) ZIF-7, and (D) ZIF-93.

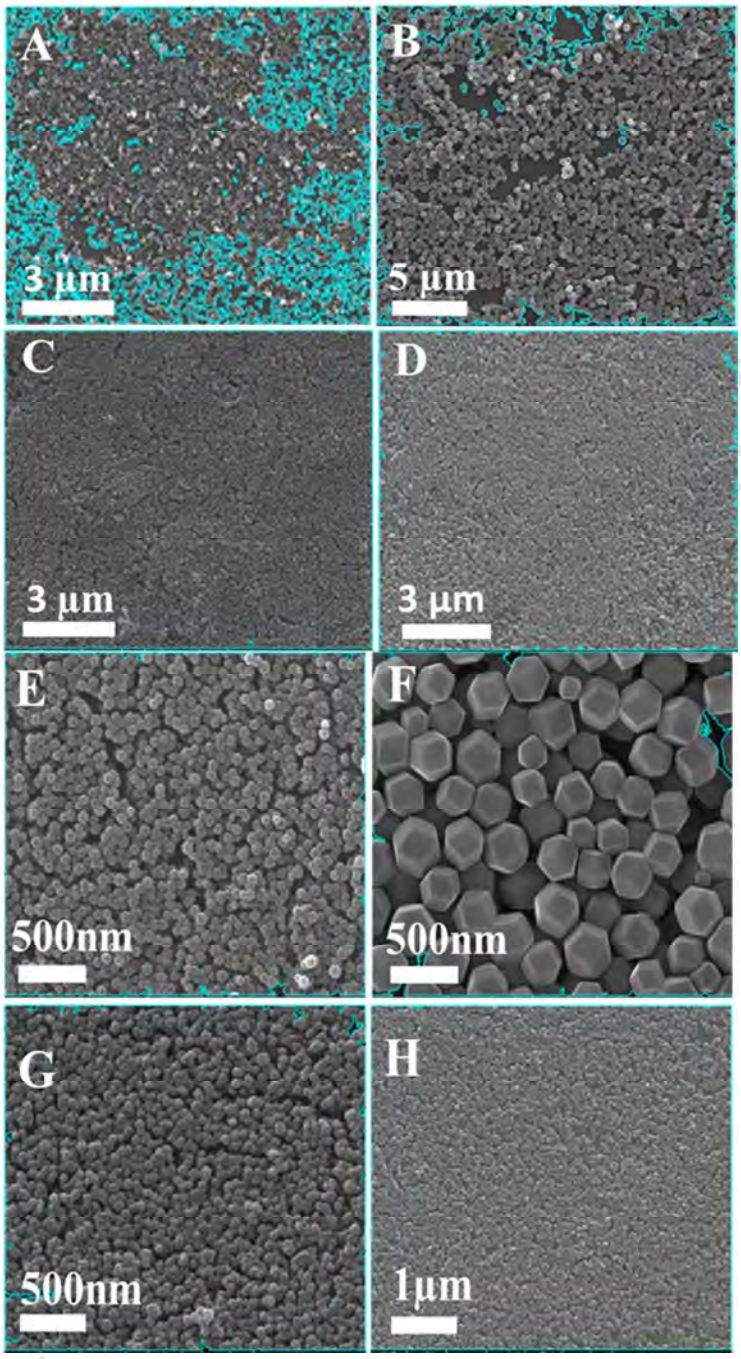

Figure S4. Images used to calculate the percentage of the coating area of ZIF films on glass substrates: (A) ZIF-8/glass_1L, (B)ZIF-67/glass_1L (C) ZIF-7/glass_1L, (D) ZIF-93/glass_1L, (E) ZIF-8/glass_2L, (F) ZIF-67/glass_2L (G) ZIF-7/glass_2L, and (H) ZIF-93/glass_2L.

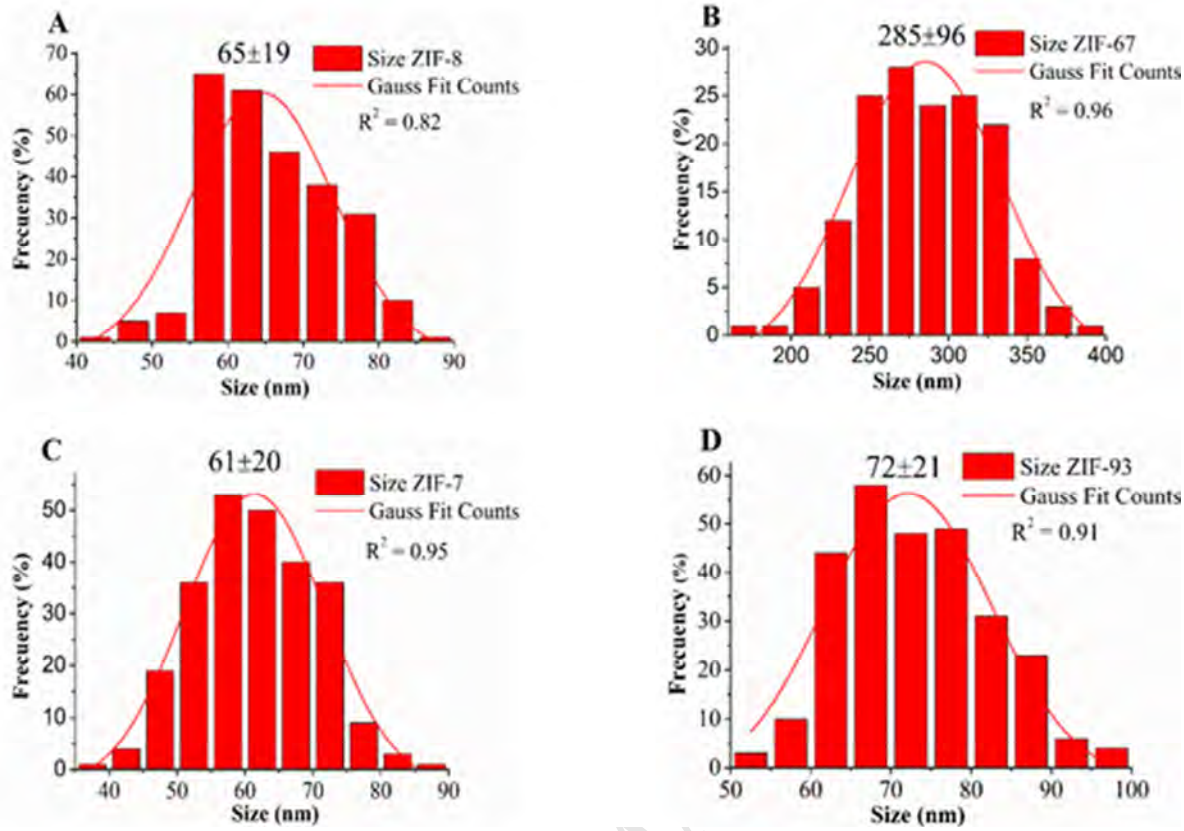

Figure S5. Particle size distributions of: (A) ZIF-8/glass, (B) ZIF-67/glass, (C) ZIF-7/glass, and (D) ZIF-93/glass.

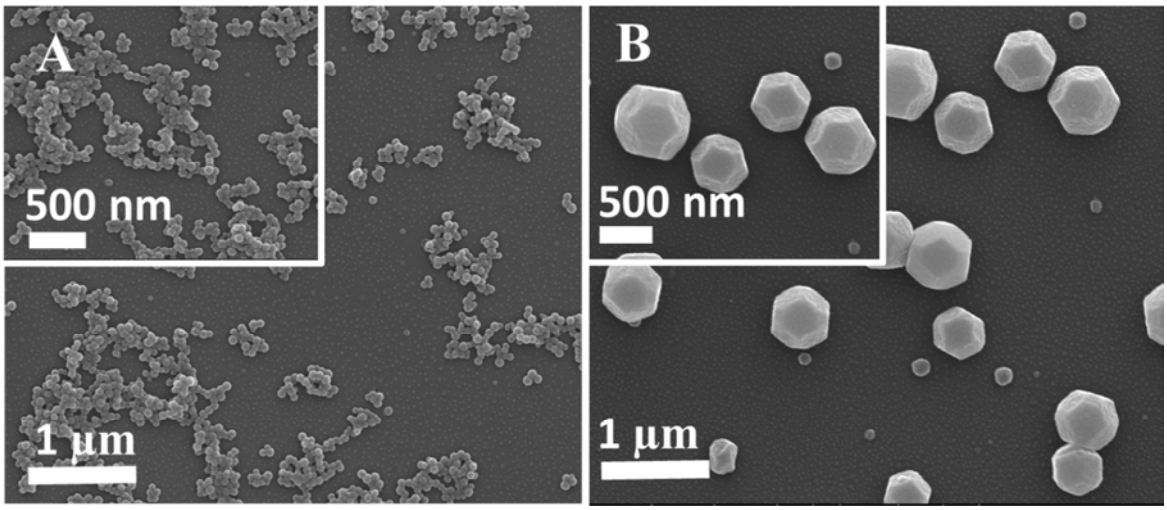

Figure S6. SEM images of ZIFs on glass substrates without functionalizing: (A) ZIF-8/glass_1L; (B) ZIF-67/glass.

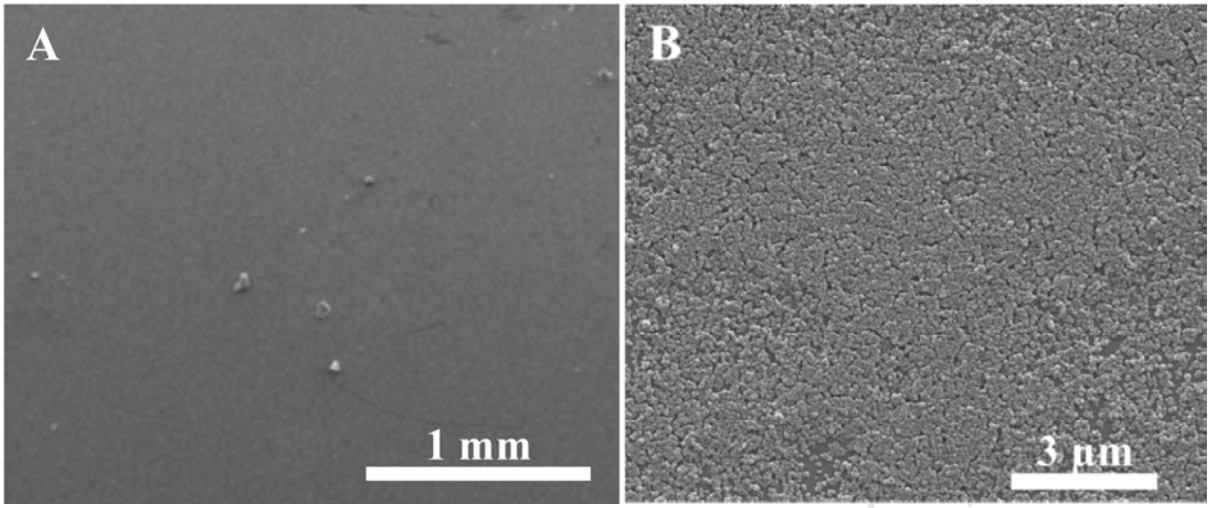

Figure S7. SEM images of ZIF-93 coatings on glass with different magnifications: (A) ca. 6 mm^2; (B) ca. 0.0001 mm^2.

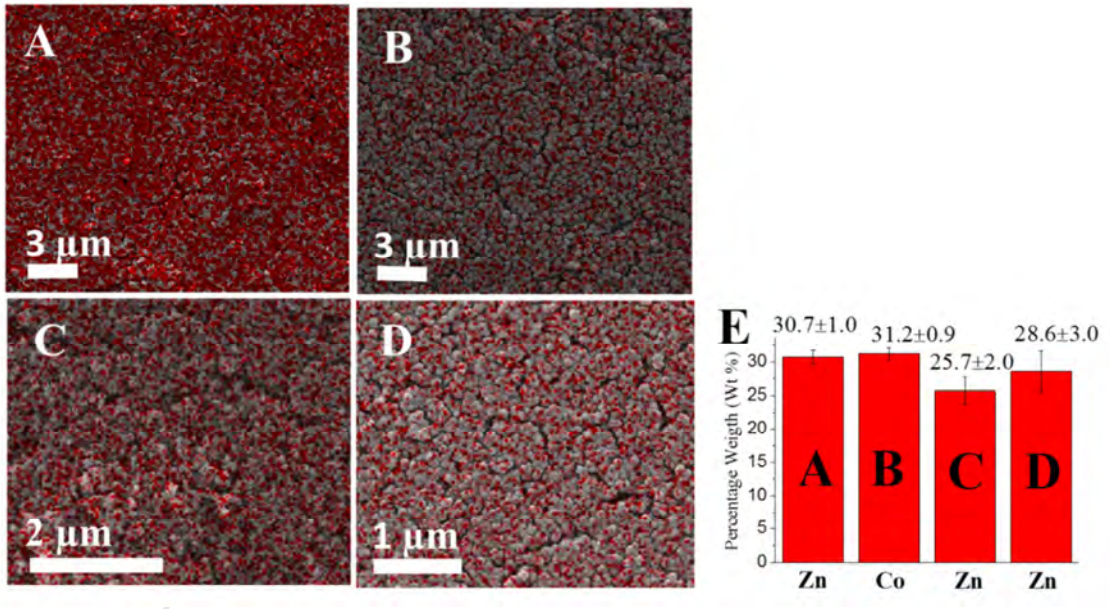

Figure S8. Zn and Co EDX mappings with spatial resolution of ca. 2-3 µm corresponding to ZIF/glass samples: (A) ZIF-8/glass_2L, (B) ZIF-67/glass_2L, (C) ZIF-7/glass_2L, (D) ZIF-93/glass_2L. The average compositions (wt%) from 3-4 different places of the same sample are shown in (E).

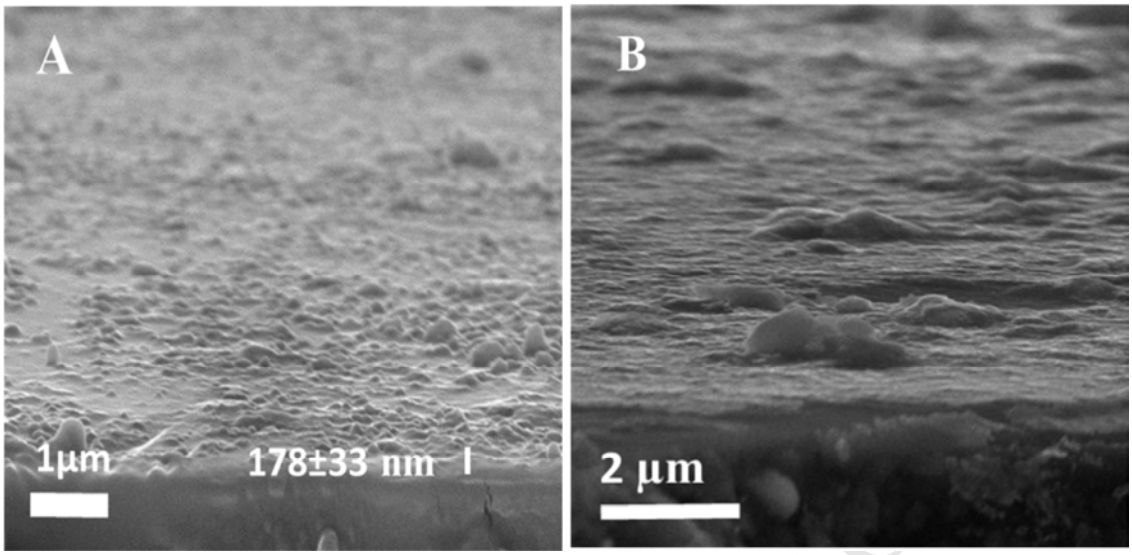

Figure S9. Cross-section SEM images of: (A) ZIF-8/glass_3L and (B) ZIF-93/glass_3L.

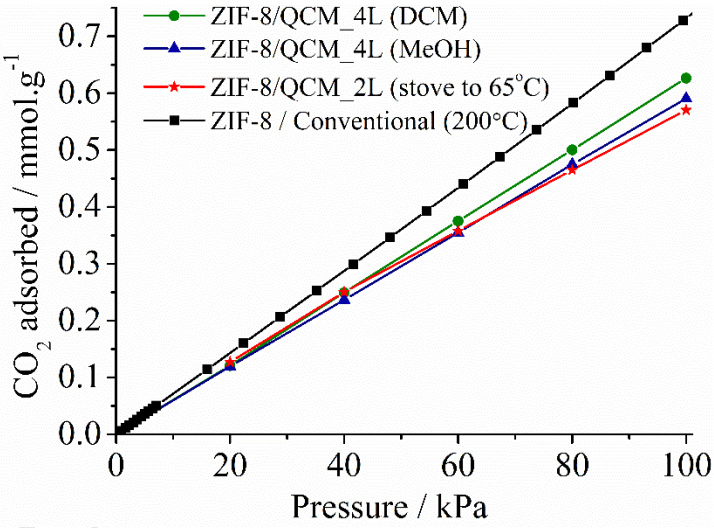

Figure S10. CO_2 adsorption isotherms at 25-30 ºC upon applying different activation methods: ZIF-8/QCM_4L (DCM), ZIF-8/QCM_4L (MeOH), ZIF-8/QCM_2L (stove to 65 ºC), ZIF-8_Conventinal (200 ºC).

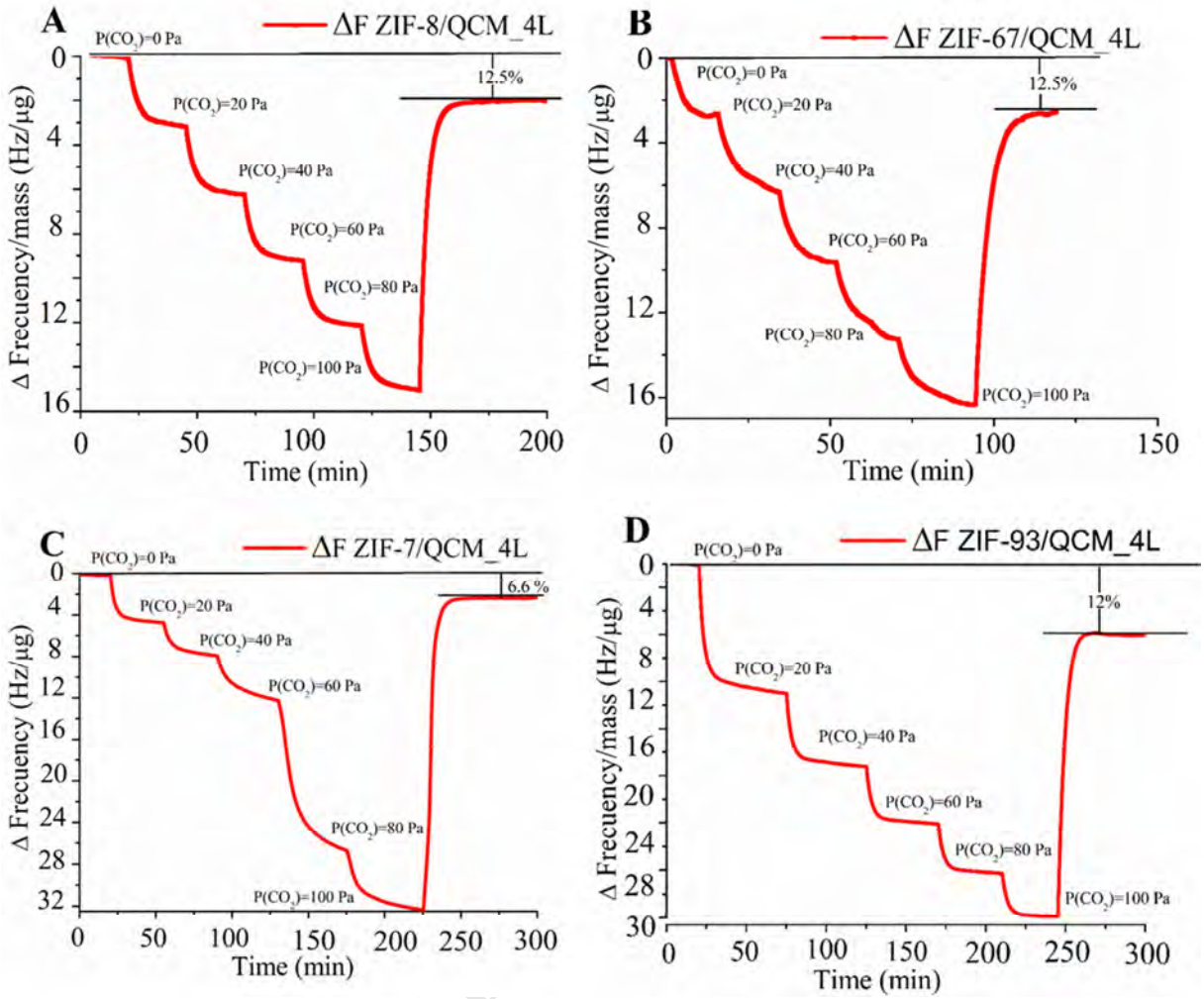

Figure S11. Resonant frequency/mass deposited as a function of time for ZIF/QCMs: (A) ZIF-8 (7 μg); (B) ZIF-67 (3 μg); (C) ZIF-7 (13 μg); and (D) ZIF-93(11 μg).